

## Detection of large thermal vibration for Cu atoms in tetrahedrite by high-angle annular dark-field imaging

Tara Prasad Mishra<sup>1</sup>, Mikio Koyano<sup>2</sup>, and Yoshifumi Oshima<sup>2\*</sup>

<sup>1</sup>Department of Materials Engineering, Indian Institute of Science, Bangalore 560012, India

<sup>2</sup>School of Materials Science, Japan Advanced Institute of Science and Technology, Nomi, Ishikawa 923-1292, Japan

\*E-mail: oshima@jaist.ac.jp

Received January 8, 2017; accepted February 21, 2017; published online March 10, 2017

Tetrahedrite ( $\text{Cu}_{12}\text{Sb}_4\text{S}_{13}$ ) is a new type of thermoelectric material with an extremely low thermal conductivity attributed to the anomalous large thermal vibration of specific Cu sites. The tetrahedrite crystal was observed from the [111] direction by high-angle annular dark-field (HAADF) imaging and the image intensity was found to be 64% lower at specific sites. This could be explained by the blurring of the intensity distribution owing to a large atomic displacement, suggesting that anomalous large thermal vibrations at specific sites in the crystal can be distinguished in HAADF images. © 2017 The Japan Society of Applied Physics

The conversion of thermoelectric (TE) energy to renewal energy is attracting increasing attention, with much effort being devoted to develop new TE materials.<sup>1)</sup> Tellurobismuthite ( $\text{Bi}_2\text{Te}_3$ ), a well-known high-TE material, has been put to practical use for TE power generation or in a Peltier cooling device. However, it is preferable to avoid bismuth (Bi) and tellurium (Te) in TE materials as they are rare elements and high in cost.

Tetrahedrite ( $\text{Cu}_{12}\text{Sb}_4\text{S}_{13}$ ) is the most important copper-containing TE mineral,<sup>2-7)</sup> as it has been suggested that its thermal conductivity ( $\kappa$ ) is suppressed by the large vibration of Cu atoms at specific sites, as determined by X-ray diffraction analysis, and the dimensionless figure of merit ( $ZT$ ) was reported to reach 0.7 with the substitution of Ni atoms.<sup>3)</sup> Tetrahedrite is a highly symmetric cubic crystal ( $I\bar{4}3m$ ) consisting of  $\text{SbS}_3$  pyramids,  $\text{CuS}_4$  tetrahedra, and unique  $\text{CuS}_3$  triangle planes [Fig. 1(a)]. In comparison with the copper atoms at the center of the  $\text{CuS}_4$  tetrahedron [denoted as Cu(1)], the Cu atoms at the center of a  $\text{CuS}_3$  triangle plane [denoted as Cu(2)] have large atomic displacement parameters (ADPs) along the plane perpendicular to the triangle plane, and have been considered to be the scattering centers of the thermal phonons. Local information, such as the scattering center, is one of the key factors in improving the performance of TE materials.

Scanning transmission electron microscopy (STEM) is a powerful tool for obtaining local structural information, and high-angle annular dark-field (HAADF) imaging is a STEM method that allows the acquisition of elemental information at individual atomic columns (Z contrast).<sup>8)</sup> Consequently, HAADF imaging is conventionally used for the identification of dopant atoms in ceramics or silicon crystals and elemental modulation at interfaces.<sup>9-12)</sup> Furthermore, HAADF imaging has the potential to identify atomic sites with the same elements but different ADPs.

Abe et al.<sup>9)</sup> found anomalous large ADPs of the Al atomic sites in the decagonal cluster of  $\text{Al}_{72}\text{Ni}_{20}\text{Co}_8$  quasicrystals.<sup>9)</sup> However, except for this study, the relationship between HAADF intensity and ADP values of individual atomic sites has rarely been reported. This may be due to the fact that the HAADF intensity depends not only on the ADP values but also on the channeling of the transmitted electron. In the double perovskite oxide of the  $\text{La}_2\text{CuSnO}_6$  crystal, the La atoms have been suggested to have different ADP values depending on their sites in the HAADF image.<sup>13)</sup> Quantita-

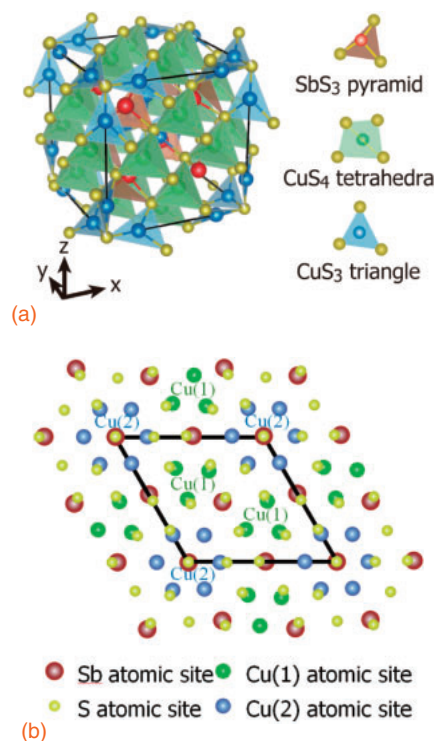


**Fig. 1.** (a) Schematic illustration of tetrahedrite crystal. The unit cell is indicated by bold lines. (b) Schematic illustration of atomic configurations of tetrahedrite crystal viewed from the [111] direction. The unit cell is indicated by a bold rhombus.

tively, ADP values were estimated by comparing the experimentally obtained HAADF image with the simulated image, but this requires the intensity distribution of the electron probe and precise sample thickness, which are difficult to obtain.<sup>14)</sup>

In this study, two different Cu atomic sites were identified with different ADPs,  $\text{CuS}_4$  tetrahedra and  $\text{CuS}_3$  triangle planes, in a tetrahedrite crystal by HAADF imaging. The Cu sites with large thermal vibrations showed lower intensities than the other Cu sites.

Tetrahedrite polycrystal ingots were synthesized by the fusion method<sup>2)</sup> and crushed in ethanol. The specimens were prepared by desiccating a drop of this suspension onto a holey carbon support film. The HAADF images were taken at the acceleration voltage of 200 kV using JEM-200F (ARM). The incident electron probe had a convergent semi-angle of 24 mrad, and the inner and outer angles for the HAADF detector

were 90 and 370 mrad, respectively. The tetrahedrite crystal was observed from the [111] direction, so that two different Cu sites were individually visible [Fig. 1(b)]. In Fig. 1(b), three Cu(1) atomic columns are located inside the triangle of three Sb atomic sites. Along these atomic columns, the Cu(1) atoms overlap with the sulfur (S) atoms, which are slightly misaligned from the row of Cu(1) atoms [noted as the Cu(1)+S atomic column]. Six Cu(2) atomic columns were located around the Sb atomic column, with three columns displaying Cu(2) atoms overlapping with the sulfur (S) atoms, which are slightly misaligned from the row of Cu(2) atoms [denoted as Cu(2)+S atomic column], and at the remaining columns, only Cu(2) atoms are aligned. The number densities of Cu(1) and Cu(2) atoms are the same among these columns.

The atomically resolved HAADF image was obtained at the edge of the wedged specimen in order to avoid the dynamical effect of the scattering electrons (see Fig. S1 in the online supplementary data at <http://stacks.iop.org/APEX/10/045601/mmedia>). From the transmission electron diffraction (TED) pattern taken from the observation area (see Fig. S2 in the online supplementary data at <http://stacks.iop.org/APEX/10/045601/mmedia>), it was found that six {440} diffracted spots had the highest intensity. The intensities decreased in the order of {440}, {220}, and {422} spots. Such an order was similar to that obtained by kinematical approximation, indicating that the sample must be very thin. By simulating the TED patterns with different thicknesses by multislice calculation, the experimental TED pattern was found to be close to the simulated pattern for a 10 nm thickness.

In order to simulate the TED patterns and HAADF images, multislice calculation was performed using the HREM<sup>TM</sup> program,<sup>15)</sup> including the absorptive potential approximation that makes use of the Weikenmeier–Kohl scattering factor. In this simulation, a lattice constant of 1.032 nm was assumed, with the fractional atomic coordinates and ADP of each atomic site taken from Pfitzner et al.<sup>16)</sup> [The ADP values of Cu(1) and Cu(2) were reported to be 2.45 and  $6.15 \times 10^{-4}$  nm<sup>2</sup>, respectively.] The convergent semi-angle and annular detector semi-angles were the same as those in the experiments. In the calculation, the reciprocal space resolution was 0.34 nm<sup>-1</sup> and the cutoff scattering vector ( $= \sin \theta_B / \lambda$ ) was set at 40 nm<sup>-1</sup> (scattering angle of 160 mrad). The defocus was chosen to be 2 nm below the top specimen surface, where the column intensity is maximum.<sup>17)</sup> To enable comparison with the experimental results, the simulated HAADF image was convolved with a Gaussian function (Fig. S3 in the online supplementary data at <http://stacks.iop.org/APEX/10/045601/mmedia>) as the experimental HAADF image was obtained with a field emission gun having a finite source (partially coherent), whereas the simulated HAADF image was obtained by assuming a point source (fully coherent).<sup>18,19)</sup> The simulated HAADF image that convolved with a Gaussian function of 100 pm at full width at half maximum (FWHM) was found to be the closest to the experimentally obtained HAADF image.

Figure 2 shows the processed HAADF image of a tetrahedrite crystal viewed from the [111] direction. It was obtained by applying the radial difference filter to the raw HAADF image (the filter passes the reciprocal information below 20 nm<sup>-1</sup> with the edge smoothed from 20 to 24 nm<sup>-1</sup>).<sup>20)</sup> In Fig. 2, the Cu(1)+S, Cu(2)+S, and Cu(2) atomic

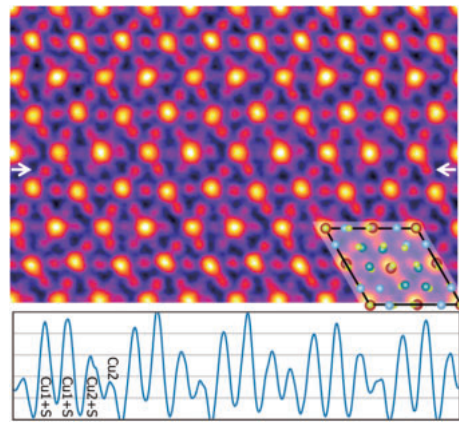


**Fig. 2.** Upper: typical HAADF image of tetrahedrite crystal viewed from the [111] direction. Lower: intensity profile along the line indicated by white arrows.

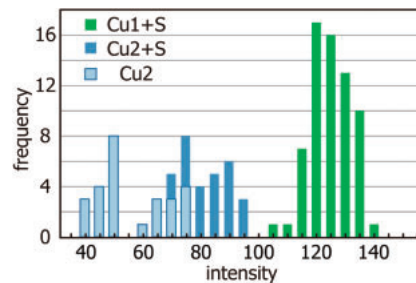


**Fig. 3.** Peak intensity histogram for Cu(1)+S, Cu(2)+S, and Cu(2) atomic columns. The average intensities were estimated to be 123, 79, and 54, respectively.

columns are clearly identified and the peaks corresponding to three neighboring Cu(1)+S, Cu(2)+S, and Cu(2) atomic columns appear periodically in the intensity profile. The three neighboring Cu(1)+S columns have different peak intensities because the overlapped S atoms are slightly misaligned, relative to each other, toward different directions from the position of Cu atoms [see Fig. 1(b)]. Obviously, the peak intensities decrease in the order of Cu(1)+S, Cu(2)+S, and Cu(2) columns. The lowest peak intensity of the Cu(2) columns can be explained by the fact that the spacing of the neighboring Cu atoms along the Cu(2) column are so large that the channeling of the transmitted electrons is relatively weak. It is not clear why the intensity of the Cu(2)+S column is lower than that of the Cu(1)+S column as the numbers of Cu and S atoms are the same in both atomic columns.

The peak intensity of each atomic column was measured by subtracting the constant background [see Fig. 4(b)] to construct the intensity histogram shown in Fig. 3. Each histogram has a certain dispersion around the mean value, which may be due to measurement error, statistical error due to a low signal-to-noise ratio, or thickness difference, for example. The mean value was estimated to be 123, 79, and 54, respectively, for Cu(1)+S, Cu(2)+S, and Cu(2) atomic columns in the histogram. The intensity ratio of Cu(2)+S to Cu(1)+S columns was determined to be 0.64 (64%).

In order to explain the intensity ratio of 0.64 (64%), five simulated HAADF images of the tetrahedrite crystal with different ADPs of the Cu(2) atomic site viewed from the [111] direction are shown in Fig. 4. The ADP of the Cu(1) atomic site was assumed to be  $2.45 \times 10^{-4}$  nm<sup>2</sup>, as reported

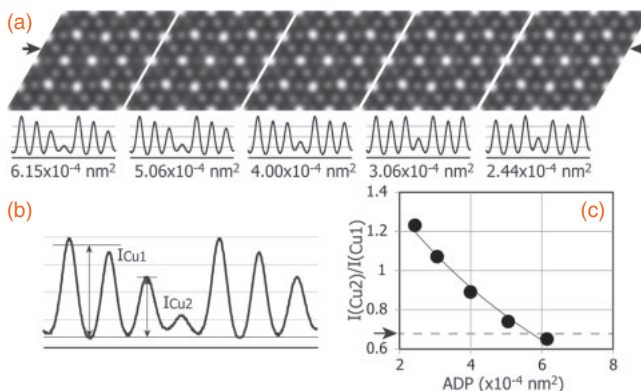


**Fig. 4.** (a) Simulated HAADF images of tetrahedrite crystal viewed from the [111] direction with different ADPs of Cu(2) atomic site. The intensity profile was obtained along the line indicated by arrows. (b) Intensity of each atomic column obtained by subtracting the constant background. The intensity of the Cu(1) atomic column was determined by averaging those of two neighboring Cu(1) atomic columns. (c) Graph of intensity ratio of  $I_{\text{Cu}2}$  to  $I_{\text{Cu}1}$  as a function of ADP of Cu(2) atomic site.

previously,<sup>16)</sup> while that of the Cu(2) atomic site was assumed to be 6.15, 5.06, 4.00, 3.06, or  $2.44 \times 10^{-4}$  nm $^2$ . In the intensity profiles in Fig. 4(a), the peak intensities of the two neighboring Cu(1)+S columns are unchanged, but that of the Cu(2)+S column decreases with increasing ADP of the Cu(2) atomic site. This indicates that the intensity ratio of Cu(2)+S to Cu(1)+S columns depends on the difference in ADP between the Cu(1) and Cu(2) atomic sites. Quantitatively, the peak intensities at the individual atomic columns were measured by subtracting the background, as shown in Fig. 4(b), and the graph of the intensity ratio of Cu(2)+S to Cu(1)+S columns was obtained as a function of the ADP of the Cu(2) atomic site [Fig. 4(c)]. In this graph, the intensity ratio exponentially decreases with increasing ADP of the Cu(2) atomic site. The experimental intensity ratio of 0.64 was found to correspond to the ADP of  $6.0 \times 10^{-4}$  nm $^2$ . Since this value is almost the same as that in the X-ray diffraction ( $6.15 \times 10^{-4}$  nm $^2$ ) results, the intensity ratio of 0.64 can be explained by the difference between the ADPs at the Cu(1) and Cu(2) atomic sites.

In this analysis, the isotropic thermal vibration of Cu(2) atomic sites was assumed since the intensity distribution of the Cu(2)+S column was almost isotropic regardless of its anisotropic thermal vibration. This isotropic intensity distribution can be explained by the Gaussian-like broadening of the electron probe. Previously, we evaluated the electron probe to be broadened similarly to a Gaussian function, with the FWHM of approximately 80 pm owing to the finite source size (partial coherent).<sup>18)</sup> The FWHM seems to be around 50 to 100 pm, depending not only on the source size but also on the probe current and/or lens aberrations. Since the FWHM is larger than the amplitude of the anisotropic thermal vibration, it is difficult to distinguish the anisotropic intensity distribution at the Cu(2) atomic column.

In general, it is difficult to distinguish either the misalignment of S atoms (channeling effect) or large ADP values as required to explain the reduction in peak intensity. However, we believe that the experimentally observed intensity difference between Cu(1)+S and Cu(2)+S atomic columns can be explained by the difference in thermal vibration between

Cu(1) and Cu(2) sites, because tetrahedrite sample used was previously confirmed by XRD analysis<sup>1,3,16)</sup> atomic coordination of Cu and S sites. In the present study, assuming isotropic thermal vibrations, the amplitude of the thermal vibration at the Cu(2) atom is estimated to be approximately 25 pm, while that at the Cu(1) atom is about 15 pm. The intensity distribution at the Cu(2)+S column must be more blurred and the peak intensity becomes lower than that at the Cu(1)+S column as a result of the larger thermal vibration.

We propose that it will be possible to distinguish either the misalignment of S atoms (channeling effect) or large ADP values if the electron probe can be made sharper by fabricating a coherent electron source and improving the lens aberration corrector. In the case of constituent atoms being exactly aligned along the column, the atomic site has been estimated with a precision of 3 to 4 pm in HAADF images.<sup>21)</sup> This suggests that the intensity distribution at the Cu+S atomic columns, consisting of misaligned S atoms, can be described by superimposing the intensity distribution of the Cu atomic site with that of the S atomic site. Also, the intensity distribution will be blurred anisotropically owing to the anisotropic thermal vibration of Cu atoms. Theoretically, from the viewpoint of each incident electron, the vibrating atoms seem to be frozen in place, since the period of atomic vibration ( $\sim 10^{-13}$  s) is much longer than the interaction time of the incident electron beam with an atom, which has been reported to be of the order of  $10^{-15}$  s on the basis of Heisenberg's uncertainty principle.<sup>22)</sup> Therefore, the HAADF image can be reproduced by summing many snapshots of the atomic structure with different atomic displacements due to thermal vibration.<sup>22)</sup> As a result, both misaligned S atoms and anisotropic ADP values may be distinguished from each other by analyzing the intensity distribution at the atomic column by STEM with an improved performance.

As mentioned above, Abe et al. found that the Al atomic sites with anomalous large thermal vibrations had higher peak intensities than the other Al sites in the quasicrystal.<sup>9)</sup> This is not in agreement with our experimental results and may be explained by the different range of annular detector angles. The inner and outer angles of the annular detector were 45 and 90 mrad, respectively, in the previous study of Abe et al., while the inner and outer angles of 90 and 370 mrad, respectively, were used in this study. At the acceleration voltage of 200 kV, the TDS cross section of the Cu atom was shown to increase with increasing ADP value below the detector angle of 50 mrad, while it was shown to be almost constant regardless of the ADP value above 50 mrad (see Fig. S4 in the online supplementary data at <http://stacks.iop.org/APEX/10/045601/mmedia>). This suggests that the decrease in peak intensity can be explained by the increase in the thermal vibration of the constituent atoms in the column, which corresponds to the ADP value, when collecting high-angle scattering electrons. Therefore, the ratio of two different ADPs can be estimated simply from the peak intensity ratio, as shown in Fig. 4(c), which is an advantage of the present experimental conditions of HAADF imaging.

In conclusion, an anomalously large vibration of the specific Cu(2) atomic sites in the tetrahedrite crystal was observed by HAADF imaging when collecting scattering electrons above 90 mrad. The peak intensity at one specific Cu column was found to be lower by 0.64 (64%) than that at the

other Cu column. The intensity ratio of 0.64 was explained by the difference in ADP between the specific and other Cu sites, and well reproduced the previous X-ray diffraction results. The simulated HAADF images showed that the peak intensity of the atomic column decreases with increasing ADP of the constituent atoms, suggesting that the amplitude of the anomalous atomic vibration can be estimated quantitatively by comparison with that of the normal atomic vibration in the same specimen; this will be helpful in the development of TE materials. Anisotropic thermal vibrations were not detected in this study because of the Gaussian-like broadening of the electron probe. Nonetheless, we will be able to distinguish an anisotropic thermal vibration directly in the HAADF image by fabricating a coherent electron source and improving the lens aberration corrector.

**Acknowledgments** We thank Professor K. Suekuni for valuable comments and Mr. T. Tsuchida and Mr. T. Nishimura for the synthesis of the tetrahedrite ingot.

- 1) S. Fujii and M. Yoshiya, *J. Electron. Mater.* **45**, 1217 (2016).
- 2) K. Suekuni, K. Tsuruta, T. Ariga, and M. Koyano, *Appl. Phys. Express* **5**, 051201 (2012).
- 3) K. Suekuni, K. Tsuruta, M. Kunii, H. Nishiate, E. Nishibori, S. Maki, M. Ohta, A. Yamamoto, and M. Koyano, *J. Appl. Phys.* **113**, 043712 (2013).
- 4) X. Lu, D. T. Morelli, Y. Xia, F. Zhou, V. Ozolins, H. Chi, X. Zhou, and C. Uher, *Adv. Energy Mater.* **3**, 342 (2013).
- 5) K. Suekuni, Y. Tomizawa, T. Ozaki, and M. Koyano, *J. Appl. Phys.* **115**, 143702 (2014).
- 6) K. Suekuni and T. Takabatake, *APL Mater.* **4**, 104503 (2016).
- 7) J. Li, M. Zhu, D. L. Abernathy, X. Ke, D. T. Morelli, and W. La, *APL Mater.* **4**, 104811 (2016).
- 8) S. J. Pennycook and D. E. Jesson, *Ultramicroscopy* **37**, 14 (1991).
- 9) E. Abe, S. J. Pennycook, and A. P. Tsai, *Nature* **421**, 347 (2003).
- 10) P. M. Voyles, D. A. Muller, J. L. Grazul, P. H. Citrin, and H. J. L. Gossman, *Nature* **416**, 826 (2002).
- 11) N. Shibata, S. J. Pennycook, T. R. Gosnell, G. S. Painter, W. A. Shelton, and P. F. Becher, *Nature* **428**, 730 (2004).
- 12) N. Shibata, S. D. Findlay, S. Azuma, T. Mizoguchi, T. Yamamoto, and Y. Ikuhara, *Nat. Mater.* **8**, 654 (2009).
- 13) M. Haruta, H. Kurata, H. Komatsu, Y. Shimakawa, and S. Isoda, *Ultramicroscopy* **109**, 361 (2009).
- 14) J. M. LeBeau, S. D. Findlay, X. Wang, A. J. Jacobson, L. J. Allen, and S. Stemmer, *Phys. Rev. B* **79**, 214110 (2009).
- 15) K. Ishizuka, *Ultramicroscopy* **90**, 71 (2002).
- 16) A. Pfitzner, M. Evain, and V. Petricek, *Acta Crystallogr., Sect. B* **53**, 337 (1997).
- 17) S. Lee, Y. Oshima, E. Hosono, H. Zhou, and K. Takayanagi, *Ultramicroscopy* **125**, 43 (2013).
- 18) S. Kim, Y. Oshima, H. Sawada, T. Kaneyama, Y. Kondo, M. Takeguchi, Y. Nakayama, Y. Tanishiro, and K. Takayanagi, *J. Electron Microsc. (Tokyo)* **60**, 109 (2011).
- 19) S. Kim, Y. Oshima, Y. Tanishiro, and K. Takayanagi, *Ultramicroscopy* **121**, 38 (2012).
- 20) K. Ishizuka, P. Eilers, and T. Kogure, *Microsc. Microanal.* **13**, 902 (2007).
- 21) A. B. Yankovich, B. Berkels, W. Dahmen, P. Binev, S. I. Sanchez, S. A. Bradley, A. Li, I. Szlufarska, and P. M. Voyles, *Nat. Commun.* **5**, 4155 (2014).
- 22) R. F. Loane, P. Xu, and J. Silcox, *Acta Crystallogr., Sect. A* **47**, 267 (1991).